Int. J. Electrochem. Sci., 12 **(2017)** 4428 – 4443, doi: 10.20964/2017.05.57

International Journal of ELECTROCHEMICAL SCIENCE
www.electrochemsci.org

Spontaneous Growth of Prussian Blue Nanoparticles on Three Dimensional Porous PEDOT for Enhanced Catalytic Reduction and Sensitive Detection of Hydrogen Peroxide

Min Yang[1], *Ying Liu*[1], *Yonggui Song*[2], *Guochun Zhao*[1], *Haiyan Tan*[1], *Qiuping Zhang*[1] *and Fugang Xu*[1,*]

[1]Key Laboratory of Functional Small Organic Molecule, Ministry of Education, College of Chemistry and Chemical Engineering, Jiangxi Normal University, 99 Ziyang Road, Nanchang 330022, China
[2]Jiangxi University of Chinese Traditional Medicine, 56 Yangming Road, Nanchang 330006, China
[*]E-mail: fgxu@jxnu.edu.cn

Received: 28 November 2016 / *Accepted:* 5 February 2017 / *Published:* 12 April 2017

In this study, a new approach was developed to prepare a novel three dimensional macroporous poly(3,4-ethylene-dioxythiophene)-Prussian blue hybrid 3D-PEDOT-PB for sensitive H_2O_2 detection. 3D-PEDOT prepared by electrodeposition not only as a conductive matrix, but also as a reductant to initiate the spontaneously "electroless" deposition of PB and as scaffold with large surface area for firmly anchoring more PB NPs. The 3D macroporous structure of the hybrid also facilitates the electron transfer and mass transport. Due to the synergistic interaction between the 3D-PEDOT and the PB NPs, the hybrid shows remarkably enhanced activity for H_2O_2 reduction. A non-enzymatic H_2O_2 sensor with a high sensitivity (981 $\mu A \cdot mM^{-1} \cdot cm^{-2}$), a wide linear range (0.17 μM to 0.257 mM) and a low detection limit (80 nM) was fabricated based on the 3D-PEDOT-PB hybrid. Furthermore, the prepared sensor displays a rapid, stable response and good selectivity. The simple preparation and advanced properties of the novel 3D-PEDOT-PB hybrid may have promising applications in electrochemical sensor, electrochromic device and so on.

Keywords: Prussian blue; hydrogen peroxide; PEDOT; electrochemical sensor; conducting polymer

1. INTRODUCTION

Prussian blue, known as an "artificial peroxidase", has received a considerable attention in the field of electrochemical sensors [1-5]. However, the intrinsic low stability and poor conductivity of PB degrade its sensing performance. It has been demonstrated that smart integration of PB with other conductive material and rational design of the synthetic procedure are effective ways to improve its stability and sensing performance [6,7].

Up to date, several conductive materials including graphene [8,9], carbon nanotubes [10] noble

nanoparticles [11] and conducting polymers [12-14] have been involved in fabricating PB based hybrids for various electrochemical sensors. Compared with carbon or noble metal materials, conducting polymer could be easily prepared with different morphologies and the redox active conducting polymers may provide new opportunities for constructing novel polymer-PB hybrids for advanced sensors. Until now, several PB-thiophene [13], PB-polypyrrole (PB-Ppy) [15] and PB-polyaniline (PB-PANI) [12,16] composite materials have been applied in electrochemical sensors, while little attention is paid on poly-(3,4-ethylenedioxythiophene) (PEDOT) [14], which has high conductivity and promising applications in electrochemical sensors, electrochromic devices and so on.

Usually, electrochemical deposition or direct chemical synthesis is employed to prepare PB or PB based nanohybrids [1,17] due to their simple operation. However, desorption of PB from electrode surface often occurs in the electrodeposition method [18], while it is hard to control the size and dispersity of PB by the direct chemical method [19]. Recently, "electroless deposition" approach is proposed for preparing PB-based hybrids [20]. In this case, the matrix itself such as carbon nanotubes, graphene, or redox-active polymer was used as the reducing reagent instead of introducing an exotic reductant. By this approach, PB could nuclear and grow firmly on the matrix, therefore an enhanced stability and improved conductivity of the hybrid are expected. Compared with carbon materials, polymers exhibit more active sites and much stronger redox activity, thus a stable anchoring and high loading of PB on the polymer matrix can be achieved to guarantee the high stability and high sensitivity of the fabricated sensor.

To improve the sensitivity of PB based sensors, the morphology of matrix to support PB is also an important issue. Due to their large surface area and porous structure for charge and mass transport in electrochemistry [21-23], three-dimensional macroporous (3DMP) films such as 3DMP PANI [21] or 3DMO Au film [22] have been used to load PB for fabricating sensitive H_2O_2 or glucose sensors. However, the preparation of these 3D porous matrixes is complex and costly. Previously, we developed a facile method to prepare a three dimensional PEDOT (3D-PEDOT) micro-nanostructure [23]. Its unique structure and strong redox activity inspired us that 3D-PEDOT should be a good matrix for fabricating PB based sensors.

In this study, a new hybrid of three dimensional macroporous 3D-PEDOT-PB was prepare by a facile combined method including electrodepositon of 3D-PEDOT and subsequent electroless growth of PB. The 3D-PEDOT not only improves the conductivity, but also initiates the electroless growth of PB, increases PB loading amount on electrode and facilitates the mass transport. The fine, well-dispersed PB grown on 3D-PEDOT provides a good and specific catalysis for H_2O_2 reduction. The synergistic interaction between PB and 3D-PEDOT framework endows the hybrid an enhanced and stable catalysis for H_2O_2 reduction. A nonenzymatic electrochemical sensor for H_2O_2 was prepared based on this 3D-PEDOT-PB hybrid, which shows high sensitivity, well stability and good selectivity.

2. EXPERIMENT

2.1. Reagents

Tetrabutyl ammonium perchlorate (TBAP), 3,4-ethylenedioxythiophene (EDOT, 97%), hydrogen peroxide (H_2O_2) and phosphate salt (NaH_2PO_4 and Na_2HPO_4) were supplied by Aladdin

chemical reagent company (Shanghai, China). Ferric chloride ($FeCl_3$), potassium ferricyanide ($K_3Fe(CN)_6$), potassium chloride (KCl), hydrochloric acid (HCl) and dichloromethane(CH_2Cl_2, 98%) were purchased from Shanghai Sinopharm Chemical Reagent Co. Ltd. (Shanghai, China). All reagents were of analytical grade. Ultra-pure water purified by a Millipore-Q System (≥18.2 MΩ cm) was used for preparing solutions except specific indication.

2.2. Preparation of 3D-PEDOT-PB hybrid

Three dimensional macroporous PEDOT (3D-PEDOT) was prepared by an electrodepostion method in a water-TBAP solution. Details can be found in our previous report [23]. Briefly, monomer solution was prepared by dissolving EDOT at a concentration of 20 mM in CH_2Cl_2 containing 100 mM TBAP as electrolyte. After that, 250 μL H_2O was added into CH_2Cl_2, and phase separation happened immediately with aqueous phase at the top. The polished glassy carbon electrode (GCE) as working electrode was immersed into the oil phase, and electrochemical deposition was carried out at 1.6 V for 60s at room temperature (25-28℃). The obtained modified electrode (3D-PEDOT/GCE) was immersed into an oxygen-free electrolyte solution (Nitrogen gas was used to degas air from the solution for 20 min) containing 1 mM $FeCl_3$, 1 mM $K_3Fe(CN)_6$, 0.025 M HCl and 0.1 M KCl. With the extension of immersion time, more and more PB NPs were deposited on the 3D-PEDOT. Typically, the immersion time was 5 min. After that, the electrode was washed with water and used for further characterization. For comparison, PB was also electrodeposited on GCE in the same solution by cyclic scanning between -0.2 V and 0.6 V with a scan rate of 50 mV/s for 10 cycles.

2.3. Apparatus

The morphology of the products were observed using an S-3400 (Hitachi, Japan) scanning electron microscope equipped with an energy-dispersive X-ray (EDS) analyzer. All electrochemical measurements were performed on a CHI 760D electrochemical workstation (Shanghai, China) using a bare or modified glassy carbon electrode (GCE, 3mm in diameter) as working electrode, a platinum wire as auxiliary electrode and a saturated calomel electrode (SCE) as reference electrode. 10 mL KCl (0.1 M, pH 3.0 tuned with diluted HCl) was used as the supporting electrolyte for electrochemical tests. The 3D-PEDOT-PB or PB modified GCE or unmodified GCE was denoted as 3D-PEDOT-PB/GCE, PB/GCE, or bare GCE, respectively. CV curves are obtained at 50mV/s, EIS results are obtained at frequency of 0.1 Hz to 10^5 Hz. Amperometric detection was operated at applied potential of 0.11 V.

3. RESULTS AND DISCUSSION

3.1 Preparation of 3D-PEDOT and 3D-PEDOT-PB hybrid

Previously, polyaniline or polypyrrole with morphologies of two dimensional film or one dimensional nanowire was used to support PB for fabricating electrochemical sensors [12-16]. Here,

another important conducting polymer PEDOT, with novel three dimensional macroporous structure (3D-PEDOT) was used as the matrix to grow PB NPs. Fig. 1a,b show the SEM images of the prepared PEDOT film. The low magnified image shows the film has many extruded tubular structures with open end (pore) of about 1 μm (Fig. 1a). Highly magnified image indicates these macropores are interconnected，which could facilitate mass transport. Moreover, lots of fiber-like structures cross-linked with each other prevail on the PEDOT film (Fig. 1b), which could act as conducting wires to accelerate the electron transfer. EDS analysis reveals the film is composed of C, O, S and Cl (Fig. 1e). This result is consistent to our previous report, indicating the robust of the method for preparation 3D-PEDOT. The unique 3D-PEDOT with macropores and nanofibers should be a good matrix for fabricating hybrid material with advanced performances.

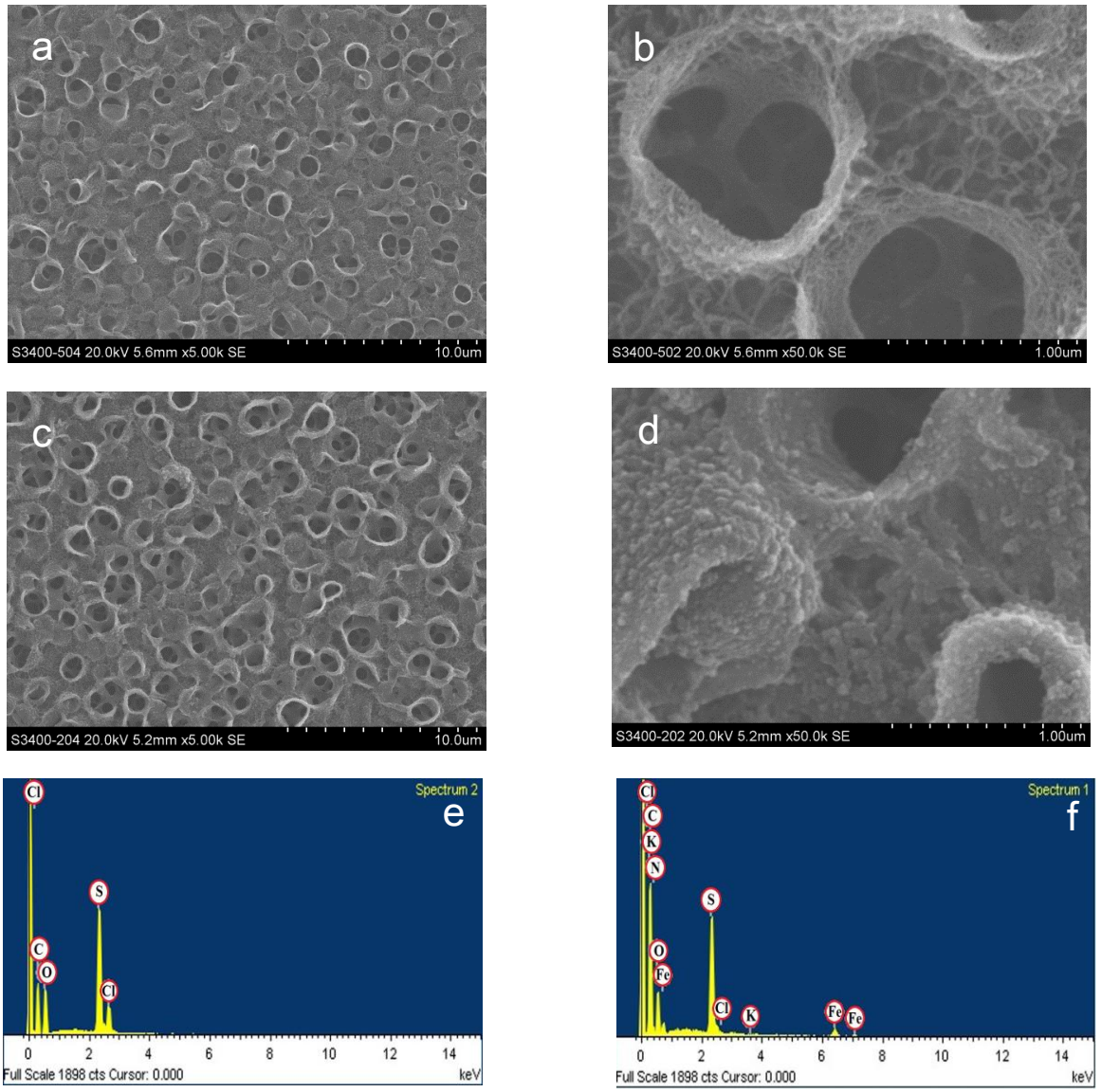

Figure 1. SEM images of 3D-PEDOT (a,b), and 3D-PEDOT-PB hybrid (c,d), and the EDS of 3D-PEDOT (e), and 3D-PEDOT-PB hybrid (f).

Next, PB was anchored on this 3D-PEDOT matrix through a spontaneous growth process. As shown in Fig. 1c,d, a layer of well-dispersed grain particles uniformly anchor on the 3D-PEDOT film. The average size of these particles is about 50 nm. Compared with PEDOT, several new elements including Fe, K, N appear (Fig. 1f). Combined the SEM, EDS and subsequent electrochemical results (Fig. 2c), it is confirmed that PB NPs is successfully anchored on PEDOT to form the three dimensional macroporous hybrid 3D-PEDOT-PB.

During preparation of the hybrid, 3D-PEDOT may have two functions. First, PEDOT as a reducing agent to reduce Fe^{3+} or $Fe(CN)_6^{3-}$ to initiate the electroless growth of PB. Control experiment revealed that almost no PB was generated on GCE within 5 min if directly immersing unmodified GCE in the growth solution of PB; Second, 3D-PEDOT could provide more active sites and large surface area to load more PB NPs with small size and improved dispersity. This was confirmed by the facts that spherical PB NPs with larger size (100 nm) and poor dispersity (aggregation happened) were formed on bare GCE if PB was electrodeposited on GCE in solution of $FeCl_3$ and $K_3Fe(CN)_6$ (Fig. S1).

3.2 Electrocatalytic reduction of hydrogen peroxide on 3D-PEDOT-PB hybrid

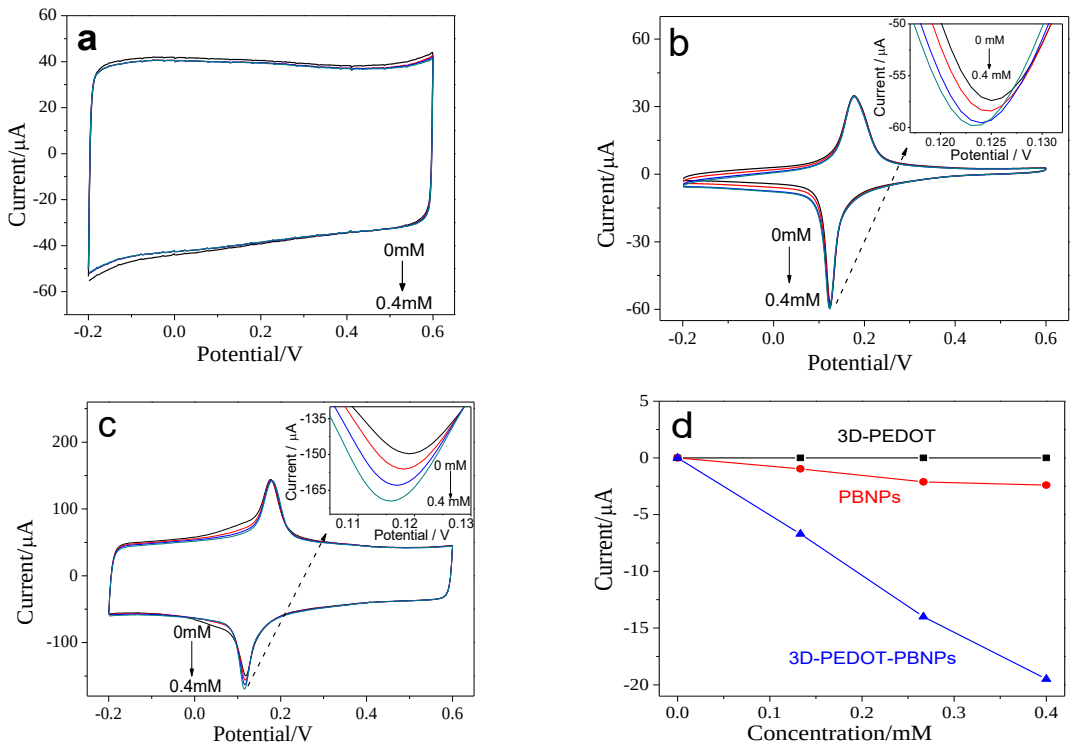

Figure 2. (a-c) Cyclic voltammetry of H_2O_2 on 3D-PEDOT/GCE(a), PB/GCE(b), and 3D-PEDOT-PB/GCE (c) in 0.1 M KCl (pH=3.0); (d) comparison the peak current response for 0, 0.13, 0.26, 0.4 mM H_2O_2 on these modified electrodes.

The as-prepared hybrid film with well dispersed, small-sized PB NPs combined with three dimensional porous PEDOT as matrix may hold great potential in different fields. Here, the activity of the 3D-PEDOT-PB hybrid film for H_2O_2 catalytic reduction was evaluated as an example of applications. Fig. 2 shows the CVs of different materials modified electrodes in the absence or presence of H_2O_2. 3D-PEDOT modified electrode (3D-PEDOT/GCE) does not show obvious peak in the presence or absence of hydrogen peroxide (Fig. 2a), indicating that PEDOT is not an active material for catalytic reduction of H_2O_2. Fig. 2b,c show that both PB/GCE (Fig. 2b) and 3D-PEDOT-PB/GCE (Fig. 2c) display the characteristic redox peaks of PB at 0.17 V and 0.11V. The electron transfer reactions may be formulated as follows [24]:

(PB) $KFe^{III}[Fe^{II}(CN)_6] + e^- + K^+ \leftrightarrow$ (PW) $K_2Fe^{II}[Fe^{II}(CN)_6]$ (1)

where PB is short for Prussian blue, PW is Prussian white.

After the injection of hydrogen peroxide, both PB/GCE and 3D-PEDOT-PB/GCE show increased reduction current at about 0.11V (Fig. 2b, c), but the increase amplitude is much larger on the later 3D-PEDOT-PB/GCE (Fig. 2d).

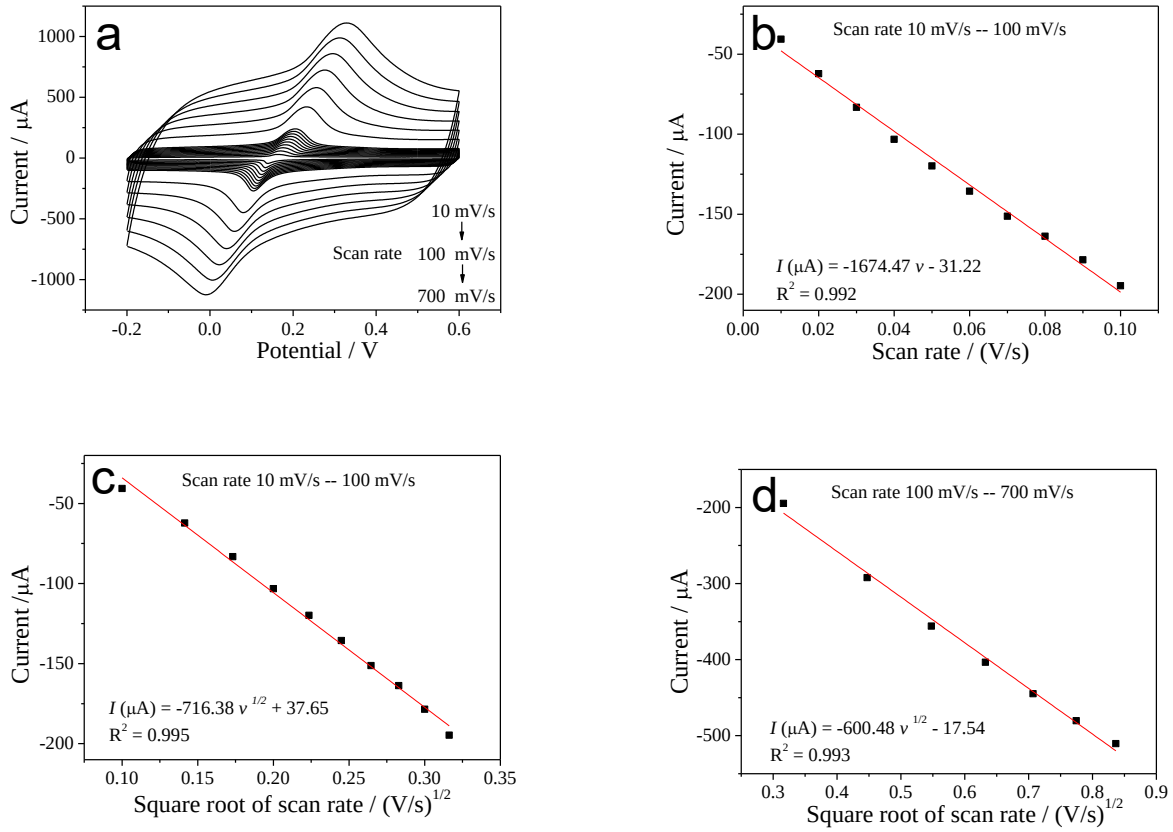

Figure 3. (a) CV curves of 0.4 mM H_2O_2 on 3D-PEDOT-PB/GCE at different scan rate (from 10 mV/s to 700 mV/s) in 0.1M KCl (pH=3.0); (b, c) the derived plot of *Peak Current* versus *Scan rate* (b) or *Peak Current* versus *square root of Scan rate* (c) at low scan rate of 10 mV/s to 100 mV/s); and (d) the derived plot of *Peak Current* versus *square root of Scan rate* at high scan rate of 100 mV/s to 700 mV/s.

As the current response obtained on 3D-PEDOT-PB/GCE is much larger than the sum value of those on PEDOT/GCE and PB/GCE (Fig. 2d), a synergistic interaction between PEDOT and PB is expected. According to published study [25], the catalytic mechanism of PB towards H_2O_2 reduction can be described as follows:

(PB) $KFe^{III}[Fe^{II}(CN)_6] + K^+ + e^- \rightarrow$(PW) $K_2Fe^{II}[Fe^{II}(CN)_6]$ (2)

(PW) $2K_2Fe^{II}[Fe^{II}(CN)_6]+H_2O_2+2H^+ \rightarrow$(PB) $2KFe^{III}[Fe^{II}(CN)_6] + 2H_2O + 2K^+$ (3)

The kinetics of H_2O_2 reduction on 3D-PEDOT-PB/GCE was further investigated by CVs at different scanning rates (Fig. 3a). The derived plots reveal the reduction peak currents display a linear dependence not only on the scan rate (Fig. 3b) but also on the square root of scan rate (Fig. 3c) when the scan rate changes from 10 mV/s to 100 mV/s. Thus it is difficult to determine the style of reaction process just according to the linear regression. Combined Fig. 3 and the results from Fig. 2, it is believed that a surface-controlled process is reasonable at this low scan rate. When the scan rate is higher than 100 mV/s, linear dependence is only established between the peak current and the square root of scan rate, indicating a diffusion controlled process. Thus, a switch of electrochemical reaction process is observed. In fact, similar switch has been reported in our previous work [26] and other papers [27,28].

Chronoamperometry can be used for the evaluation of the catalytic rate constant with the help of the following equation [29].

$$\frac{I_{cat}}{I_d} = \lambda^{0.5}\left[\pi^{0.5} erf\left(\lambda^{0.5}\right) + \frac{\exp(-\lambda)}{\lambda^{0.5}}\right] \quad (4)$$

In the case where λ>1.5, $erf(\lambda^{0.5})$ is almost equal to unity. Then the above equation can be reduced to:

$$\frac{I_{cat}}{I_d} = \lambda^{0.5}\pi^{0.5} = \pi^{0.5}\left(K_{cat}Ct\right)^{0.5} \quad (5)$$

where I_{cat} and I_d are the current in the presence or absence of analyte; k_{cat} is the catalytic rate constant ($M^{-1}s^{-1}$); C is analyte concentration (M), and t is time elapsed (s). Fig. 4a shows the current responses obtained on 3D-PEDOT-PB/GCE in the absence or presence of different concentrations of H_2O_2 at fixed potential step 0.11 V. The current steadily increases as more H_2O_2 was added. The derived plot of I_{cat}/I_d versus $t^{1/2}$ exhibits a linear relationship as shown in Fig. 4b, which can be fitted by the above equation (5). Through this equation, the k_{cat} for H_2O_2 reduction on 3D-PEDOT-PB/GCE is calculated as 1.37×10^6 $M^{-1}s^{-1}$. For comparison, the chronoamperometry curve obtained on PB/GCE was also recorded (Fig. 4c), and its derived plot is shown as Fig. 4d. The k_{cat} obtained on PB/GCE is calculated as 1.24×10^5 $M^{-1}s^{-1}$. Obviously, the k_{cat} of 3D-PEDOT-PB is about 11-fold of that obtained on PBNPs, further confirming the enhanced catalysis of the 3D-PEDOT-PB hybrid.

These results from CV and chronoamperometry clearly demonstrate that introducing 3D-PEDOT into the hybrid film largely improves the catalysis for H_2O_2. The reasons can be ascribed to the following factors. (1) Large surface area: 3D-PEDOT with three-dimensional porous structure have large surface area.

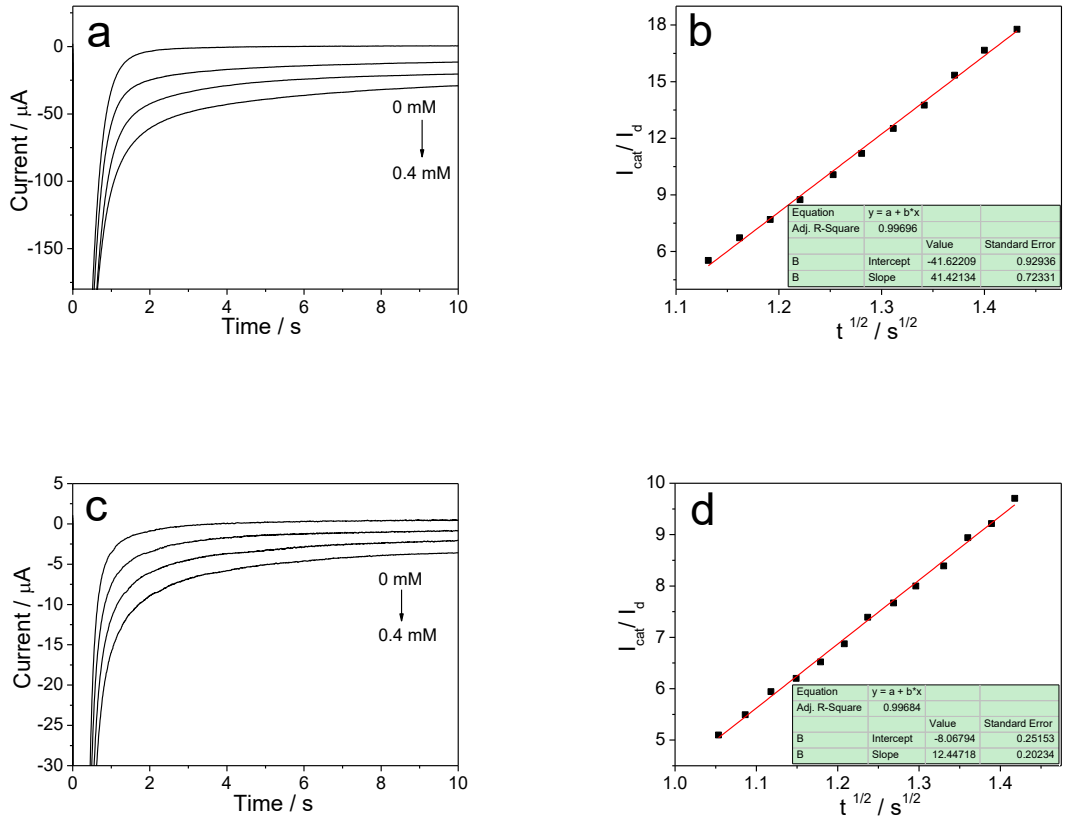

Figure 4. (a, c) Chronoamperometric response on 3D-PEDOT-PB/GCE (a) or PB/GCE (c) in the presence of 0, 0.13, 0.26, 0.4 mM of H_2O_2 at potential of 0.11 V. (b, d) The plot of I_{cat}/I_d versus $t^{1/2}$ for 3D-PEDOT-PB/GCE (b), or PB/GCE (d) for 0.4 mM H_2O_2.

The unique structure could provide more active sites for growing well-dispersed, fine PB with enhanced catalysis compared to the aggregated PB on bare GCE. This has been confirmed by SEM results in Fig.1 and Fig. S1. (2) Improved conductivity: The high frequency part of EIS curve of the 3D-PEDOT-PB/GCE shows a much small diameter than that of PB/GCE (Fig. 5), indicating that the 3D-PEDOT-PB hybrid has lower resistance (~5 Ω) of charge transfer than that of PB/GCE (~ 73 Ω). This can be ascribed to the abundant nanofibers on PEDOT, which act as conducing wires to cross-link PB to improve the conductivity of the hybrid. (3) Enhanced mass transport: The slope of the linear part of EIS curve of 3D-PEDOT-PB/GCE is greatly larger than that of PB/GCE (Fig. 5), indicating an improved efficiency of mass transport. The macro-holes of 3D-PEDOT could facilitate H_2O_2 to pass through and be reduced at the electrode catalyzed by PB [21-23].

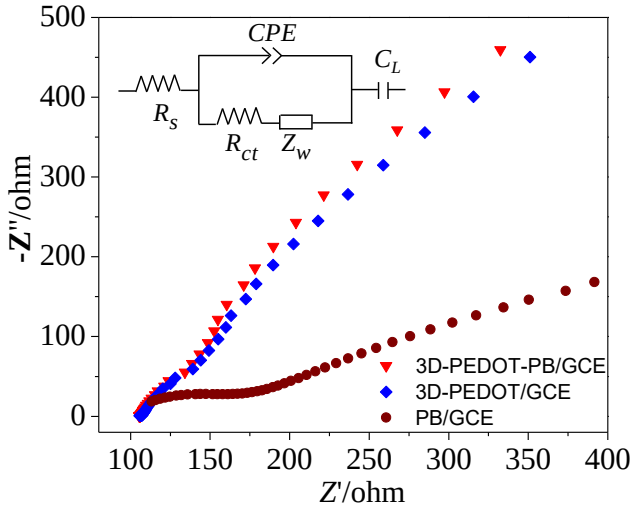

Figure 5. EIS measurement results of PB/GCE, 3D-PEDOT/GCE, and 3D-PEDOT-PB/GCE in 5 mM $K_3Fe(CN)_6$-$K_4Fe(CN)_6$ in the presence of 0.1M KCl. Inset is the equivalent circuit.

3.3 Effect of immersion time on hydrogen peroxide reduction

In our method, PEDOT is used not only as a conductive matrix, but also as a reductant to initiate the growth of PB, and thus the reaction time of PEDOT with PB precursor (i.e., the immersion time of PEDOT in PB precursor) should be a critical parameter for controlling the size or morphology of PB NPs and its electrochemical activity. Fig.S2 shows the morphology of 3D-PEDOT-PB hybrid obtained at different immersion time. As the immersion time increases, more and more PB NPs grow on 3D-PEDOT. The porous and fibrous structures of PEDOT are still clearly seen within 10 min (Fig.S2a-d). However, when the immersion time is over 10 min, there are too many PB NPs grown on PEDOT, which lead to the aggregation of PB NPs and complete cover of PEDOT fibrous structures (Fig.S2e-g). That will result in low active surface area and poor conductivity. Thus, too long immersion time may reduce the catalytic property of the hybrid material. This hypothesis was confirmed by the electrochemical measurement. Fig.S3a shows the catalytic peak potential and peak current of H_2O_2 obtained on the 3D-PEDOT-PB produced with different immersion time. As the immersion time elongates, the value of reduction peak potential gradually decreases. For the reduction peak current, it first grows and then decreases, and the maximum current response is obtained on 3D-PEDOT-PB with 5 min growth time. To achieve a high sensitivity for H_2O_2 detection, 3D-PEDOT-PB produced from 5 min growth was chosen to do the following experiments.

3.4 Effect of pH on hydrogen peroxide reduction

Previous work indicates the pH value of the electrolyte has important effect on the electrochemical activity of PB [30, 31]. Here, catalysis activity of PB for H_2O_2 in phosphate buffers with pH from 2.0 to 6.0 were tested. Fig.S3b shows the variation of peak position and peak current response of 3D-PEDOT-PB/GCE in PBS with different pH values. The peak potential only slightly

fluctuates between 0.11 V and 0.12 V as solution pH increases. However, the current response shows an obvious change, which increases as pH changes from 2 to 3, and then sharply decreases when pH is further elevated. The reason can be ascribed to the intrinsic poor stability of PB in neutral and alkaline solutions and PW is slightly soluble in alkaline conditions [31, 32]. Results from amperometric test in Fig. S4 also indicate the 3D-PEDOT-PB/GCE shows larger and more stable current response at pH 3.0 than those obtained at other pH values. Therefore, 0.1M KCl solution with pH 3.0 (tuned with diluted HCl) was used as the electrolyte in the following measurement.

3.5 Amperometric detection of hydrogen peroxide

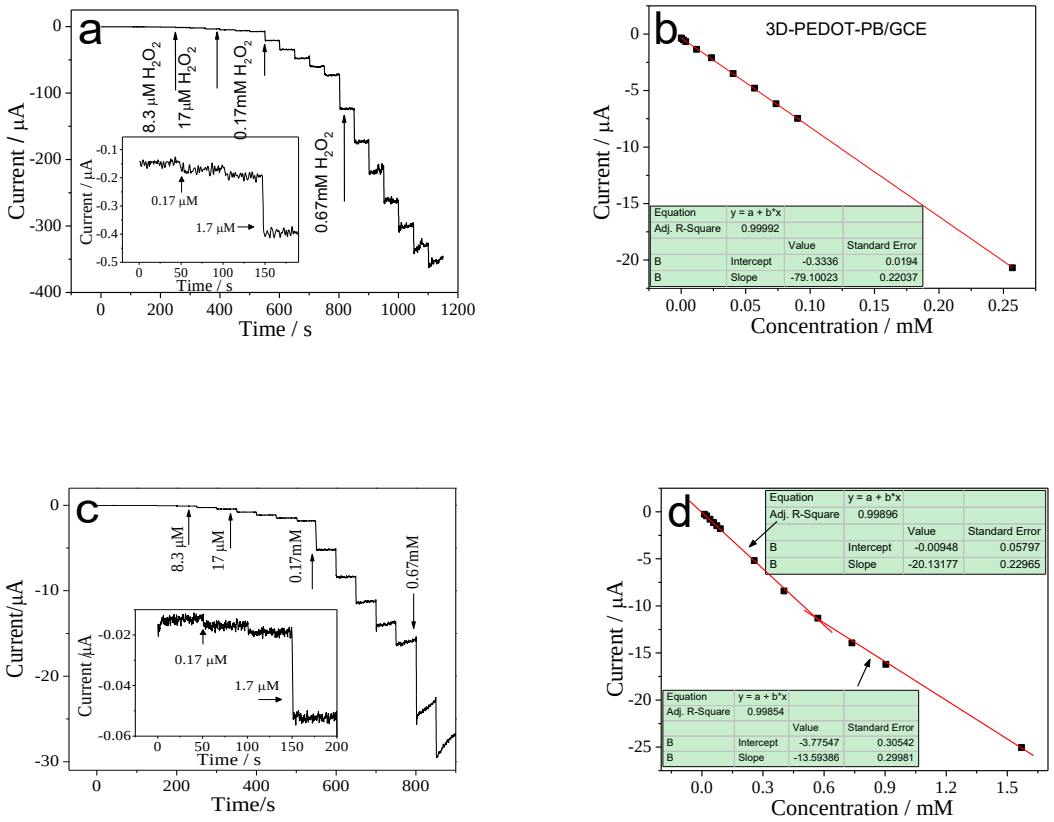

Figure 6. Amperometric curve (a, c) and calibration plot of current versus concentration (b, d) for the detection of H_2O_2 on 3D-PEDOT-PB/GCE (a, b) or PB/GCE (c, d) in 0.1 M KCl (pH=3.0). Applied potential: 0.11V.

The analytical performances of the sensor toward H_2O_2 reduction were further investigated using amperometric technique under the optimum conditions (0.1 M KCl, pH=3, applied potential of 0.11 V). Fig. 6a shows the 3D-PEDOT-PB/GCE displays a fast and strong current response upon the addition of H_2O_2. The current displays a linear dependence on the concentration of H_2O_2 in the range of 0.17 μM to 0.257 mM, and a polynomial dependence is established at high concentration H_2O_2 from

0.257 mM to 5.57 mM (Fig. S5). A detection limit of 80 nM was obtained on this 3D-PEDOT-PB/GCE according to the linear calibration curve (Fig. 6b). Instead, PB/GCE shows a relative lower current response (Fig. 6c), with two linear response ranges of 12.0 μM to 0.570 mM and 0.570 mM to 1.57 mM (Fig. 6d). A detection limit of 3.0 μM is obtained on PB/GCE based on the first linear range.

Table 1. Electroanalytical characteristics of various modified electrodes toward H_2O_2

Material	Sensitivity ($\mu A \cdot mM^{-1} \cdot cm^{-2}$)	Linear range (mM)	Detection limit (μM)	Reference
PB-RGO	196.6	0.02 -0.2	1.9	33
PB-FCNFs	62.35	0.004 - 25	0.7	34
PB-PANI-HNTs	980	0.004 -1.1	0.226	35
PB-TiO_2/ITO	30	0.1 -1.4	0.42	36
PB-RTIL-CNFs	185.9	0.00049 -0.7	0.49	37
PB-GO	408.7	0.005 -1.2	0.122	38
PB-MCNTs	153.7	0.010 – 0.4	0.567	39
PB-RGO	20	1 -7	5	40
PB-rGO-CS	816.4	0.01 -0.4	0.213	41
PB-AuNPs/TiNTs	1100	0.003-1.1	1.0	42
PB/MPS/Au	48.79	0.002-0.2	1.8	43
PEDOT-PBNPs	981	0.00017-0.257	0.08	This work

Compared with PB, the H_2O_2 sensor based on 3D-PEDOT-PB displays a higher sensitivity, wider linear range and lower detection limit due to the aforementioned synergistic interaction between 3D-PEDOT and PB. This performance of the 3D-PEDOT-PB sensor is comparable or even better than many previously reported H_2O_2 sensors based on PB (Table 1), which further demonstrates the advantage of introducing 3D-PEDOT into this sensor.

3.6 Interference studies, repeatability and stability

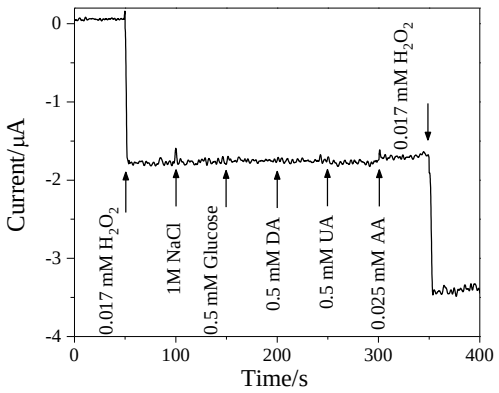

Figure 7. Amperometic response for H_2O_2 and other concomitant molecules obtained on 3D-PEDOT-PB/GCE. Applied potential: 0.11 V.

To study the selectivity of the 3D-PEDOT-PB/GCE for H_2O_2 detection, the amperometric responses of the sensor for H_2O_2 and other potential interfering species were investigated. The results in Fig. 7 show that 30-fold of uric acid (UA), dopamine (DA), glucose (Glu), 60-fold concentrations of NaCl and 1.5-fold concentrations of ascorbic acid (AA) display negligible response compared with that of 0.017 mM H_2O_2, which indicates a good selectivity. For five successive amperometric measurements of 0.35 mM H_2O_2, a relative standard deviation value (RSD) of 4.8% was obtained for the steady current response. After storage in air at room temperature for a month, the 3D-PEDOT-PB/GCE still shows 95% value of the original current response for the same concentration of H_2O_2, indicating a good stability.

4. CONCLUSIONS

In summary, a new three dimensional, macro-porous hybrid of 3D-PEDOT-PB was prepared through an electrodeposition combined electroless growth approach. The 3D-PEDOT exhibits multifunction in this hybrid: reducing agent to initiate PB growth, anchoring matrix with large surface area for elevating PB loading, improving the conductivity of the hybrid, and facilitating the charge transfer and mass transport. Due to the synergistic interaction between 3D-PEDOT and PB, the 3D-PEDOT-PB hybrid exhibited enhanced catalysis for H_2O_2 reduction, and a rapid, stable and sensitive H_2O_2 sensor was fabricated based on the 3D-PEDOT-PB hybrid. Our results indicate the 3D-PEDOT-PB hybrid film may serve as a platform for the detection of hydrogen peroxide in the development of a variety of bioelectrochemical sensors or devices.

SUPPORTING MATERIAL:

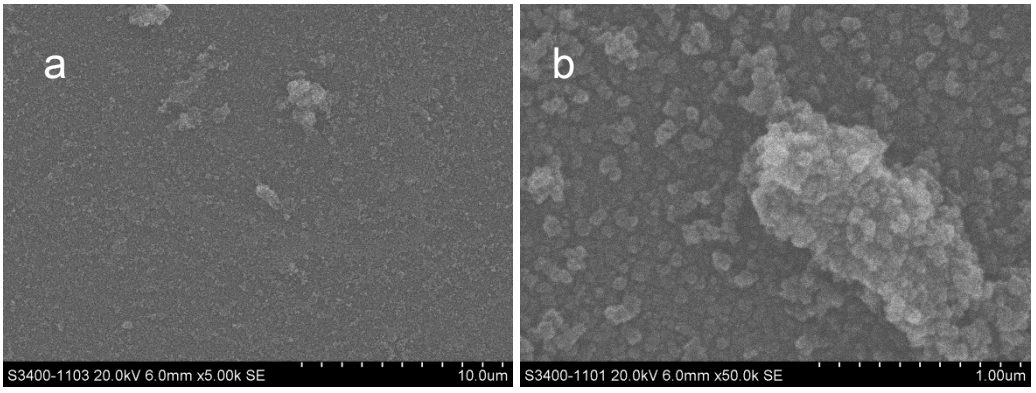

Fig. S1 SEM images of PB NPs deposited on bare GCE.

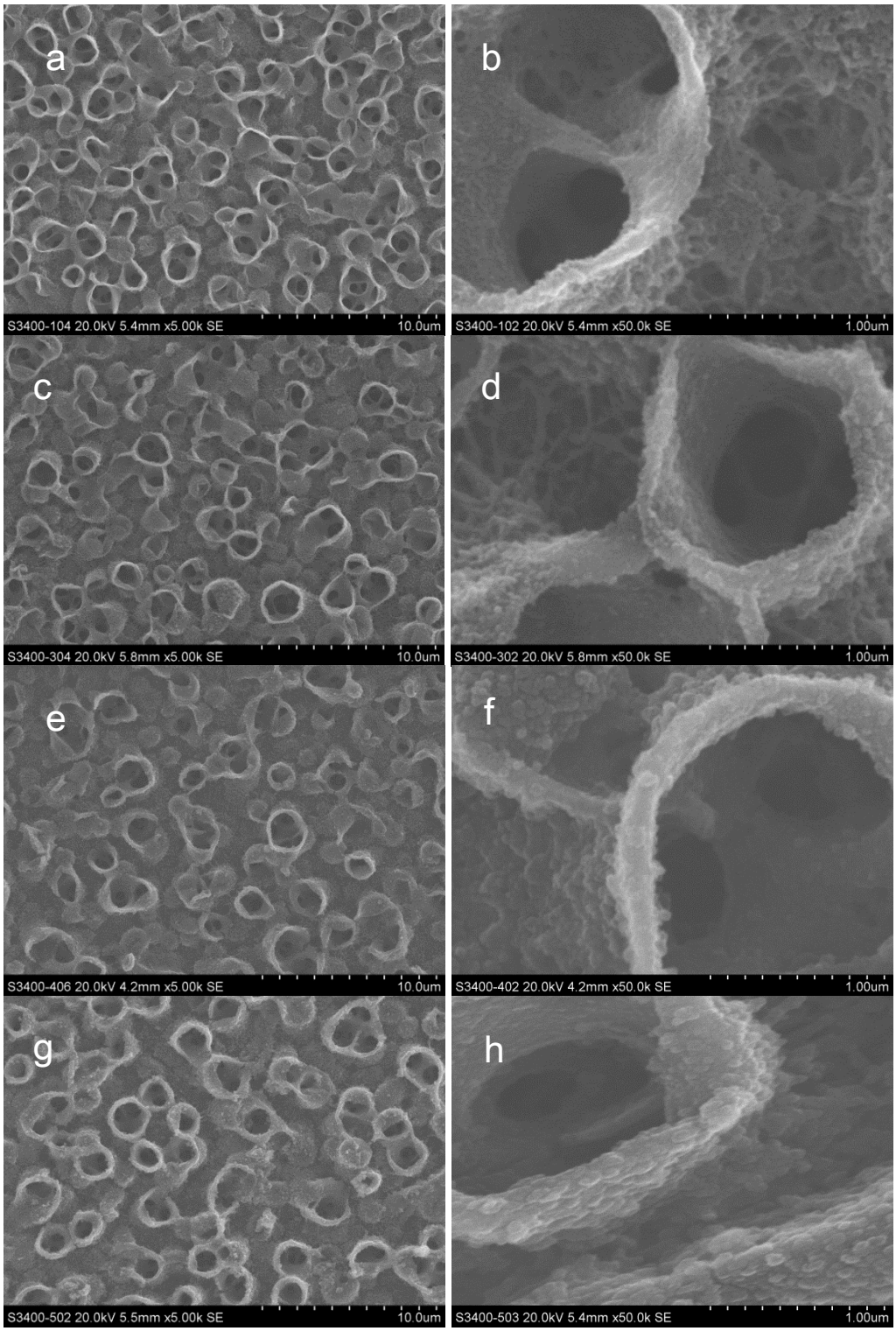

Fig. S2 SEM images of 3D-PEDOT-PB hybrid with different immersion time: (a,b) 1 min; (c,d) 3 min; (e,f)10 min; (g,h) 20 min.

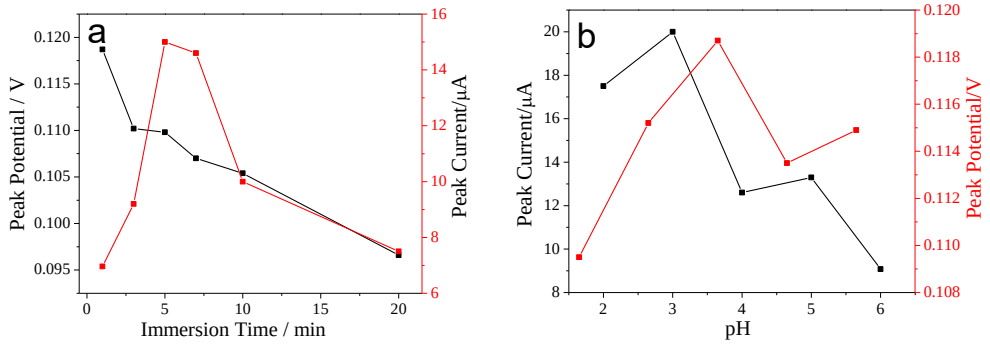

Fig. S3 (a) The variation of peak potential and peak current of 0.13 mM H_2O_2 obtained on 3D-PEDOT-PB/GCE with PB grown at different immersion time; (b) the peak potential and peak current of 0.13 mM H_2O_2 on 3D-PEDOT-PB/GCE in PBS with different pH.

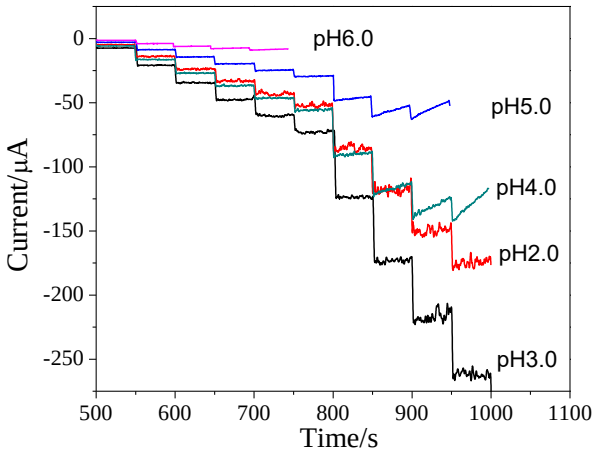

Fig. S4 Amperometric response of H_2O_2 obtained on 3D-PEDOT-PB/GCE in PBS (containing 0.1M KCl) solution with different pH values. Applied potential: 0.11V.

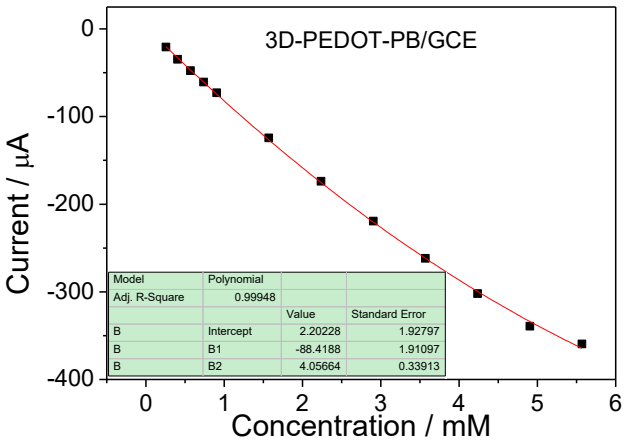

Fig. S5. The polynomial fitting curve for current response versus concentration of H_2O_2 for 3D-PEDOT-PB/GCE in the concentration range of 0.257 mM to 5.57 mM.

ACKNOWLEDGEMENT
This work is financially supported by the Natural Science Foundation of China (21665011), Science Foundation from Jiangxi Provincial Department of Education (GJJ14263), Scientific Research Funds of Jiangxi Normal University (No.4506 and No. 4304), and Open Project Program of Key Laboratory of Functional Small Organic Molecule, Ministry of Education, Jiangxi Normal University (No. KLFS-KF-201428).

References

1. B. Kong, C. Selomulya, G. F. Zheng, D. Y. Zhao, *Chem. Soc. Rev.*, 44(2015)7997
2. Y. J. Dong, S. C. Zhao, Z. M. Li, H. Yue, Y. Wang, L. G. Deng, S. Q. Zhang, *Inter. J. Electrochem. Sci.*, 11(2015)1765
3. C. Zhai, X. Sun, W. Zhao, *Biosens. Bioelectron.*, 42(2013)124
4. A. S. Adekunle, O. A. Arotiba, B. B. Mamba, *Inter. J. Electrochem. Sci.*, 11(2015)1765
5. L. F. Sgobbi, C. A. Razzino, S. A. S. Machado, *Electrochim. Acta*, 191(2016) 1010
6. L. Chen, X. Wang, X. T. Zhang, H. M. Zhang, *J Mater Chem.*, 22(2012)22090
7. B. Haghighi, S. Varma, *Talanta*, 64 (2004) 3
8. Y. L. Cao, Y. L. Liu, B. H. Zhang, L. H. Lu, *ACS Appl Mater Inter.*, 8(2010)2339
9. R. X. Chen, Q. P. Zhang, Y. Gu, L. Tang, C. Li, Z. Q. Zhang, *Anal. Chim. Acta*, 167(2015) 1280
10. S. Husmann, E. Nossol, A. J. G.Zarbin, *Sens Actuators B: Chem.*, 192(2014)782
11. I. L. Mattos, L. Gorton, T. Ruzgas, *Biosens Bioelectron.*, 18(2003)193
12. B. Thakur, S. N. Sawant, *ChemPlusChem.*, 78(2013)166
13. L. Guadagnini, E. Salatelli,A. Kharina, D. Tonelli, *J. Solid State Electrochem.*, 18(2014)2731
14. S. Lupu, B. Lakard, J. Y. Hihn, *Thin Solid Films.*, 519(2011)7754
15. H. Zhao, Y. Yuan, S. Adeloju, G. G. Wallace, *Anal Chim Acta.*, 472(2002)113
16. L. Zhou, S. Wu, H. Xu, *Anal. Meth.*, 6(2014)8003
17. P. Najafisayar, M. E. Bahrololoom, *Thin Solid Films.*, 542(2013)45
18. Y. J. Zou, J. Cheng, C. L. Xiang, H. L. Chu, S. J. Qiu, F. Xu, L. X. Sun, L. J. Zheng, *Inter. J. Electrochem. Sci.*, 10(2015)4626
19. N. V. Talagaeva, E. V. Zolotukhina, I. Bezverkhyy, D. V. Konev, Y. Lacroute, E. Y. Maksimova, S. L. Koryakin, M. A. Vorotyntsev, *J. Solid State Electrochem.*, 19 (2015)2701
20. L. Wang, S. Tricard, P. W. Yue, J. H. Zhao, J. Fang, W. G. Shen, *Biosens. Bioelectron.*, 77(2016)1112
21. X. J. Chen, Z. X. Chen, R. Tian, W. Yan, C. Yao, *Anal. Chim. Acta.*, 723(2012)94
22. J. Yang, M. Lin, M. Cho, Y. Lee, *Microchim. Acta.*, 182(2015)1089
23. F. Xu, Y. Liu, G. Ding, *Electrochim. Acta.*, 50(2014)223
24. P. Salazar, M. Martín, F. J. García-García, *Sens. Actuators B: Chem.*, 213(2015)116
25. Y. Zhang, J. Xie, *Anal. Meth.*, 6(2014)9761
26. F. G. Xu, M. Deng, G. Y. Li, S. H. Chen, L. Wang, *Electrochim. Acta.*, 88(2013)59
27. S. Li, Y. Zheng, G. W. Qin, Y. Ren, W. Pei, L. Zuo, *Talanta.*, 85(2011)1260
28. S. Hou, M. L. Kasner, S. Su, K. Patel, R. Cuellari, *J. Phys. Chem C.*, 114(2013)14915
29. A. J. Bard, L. R. Faulkner, *Electrochemical Methods*, John Wiley and Sons, (2001) New York, USA.
30. F. Ricci, G. Palleschi, *Biosens. Bioelectron.*, 45(2005)389
31. A. A. Karyakin, *Electroanalysis.*, 13(2001)813
32. R, Koncki, *Critical Rev. Anal. Chem.*, 32(2002)79
33. E. Jin, X. Lu, L. Cui, *Electrochim. Acta.*, 55(2010)7230
34. L. Wang, Y. Ye, H. Zhu, *Nanotech.*, 23(2012)455
35. Q. Sheng, D. Zhang, Q. Wu, *Anal. Meth.*, 7(2015)6896

36. M. Gaitán, V. R. Gonçales, *Biosens. Bioelectron.*, 26(2010)890
37. A. H. Keihan, S. Sajjadi, *Electrochim. Acta.*, 113(2013)803
38. Y. Zhang, X. Sun, L. Zhu, *Electrochim Acta.*, 56(2011)1239
39. J. Zhai, Y. Zhai, D. Wen, *Electroanalysis.*, 21(2009)2207
40. N. Zhu, S. Han, S. Gan, *Adv. Func. Mater.*, 23(2013)5297
41. J. H. Yang, N. Myoung, H. G. Hong, *Electrochim. Acta.*, 81(2012)37
42. Z. D. Gao, Y. Y. Han, Y. C. Li, M. Yang, Y. Y. Song, *Electrochim. Acta.*, 125(2014)530
43. Y. Zhang, H. Q. Luo, N. B. Li, *Bioprocess Biosyst. Eng.*, 34(2011)215